

Thermodynamic study of non-solvent/dimethyl sulfoxide/polyacrylonitrile ternary systems: effects of the non-solvent species

Jian Zhang · Youwei Zhang · Jiongxin Zhao

Received: 17 May 2010 / Revised: 22 April 2011 / Accepted: 29 May 2011 /

Published online: 4 June 2011

© Springer-Verlag 2011

Abstract In order to investigate the effects of the non-solvent species on the formation mechanism of polyacrylonitrile (PAN) fiber in wet spinning, theoretical ternary phase diagrams of water/DMSO/PAN and ethanol/DMSO/PAN systems were constructed based on the extended Flory–Huggins theory. The cloud-points of dilute PAN solutions of the two systems were determined by titration method and those of concentrated PAN solutions from Boom's linearized cloud-point correlation. Binary interaction parameters were calculated and optimized to construct the theoretical phase diagram. The obtained diagrams were used to investigate the effects of the non-solvent species on the formation of PAN fibers. If the non-solvent water is replaced with ethanol, the meta-stable two-phase region in the ternary phase diagram increases. This favors the de-mixing of the filament via nucleation and growth mechanism during the coagulation process, resulting in homogenous dense PAN fibers with low porosity.

Keywords Phase diagrams · Fibers · Morphology · Non-solvent · Polyacrylonitrile (PAN)

List of symbols

$a, b, a_0, a_1, a_2, a_3, a_4, \alpha$	Constants
w_1	Mass fraction of non-solvent
w_2	Mass fraction of solvent
w_3	Mass fraction of polymer

J. Zhang · Y. Zhang (✉) · J. Zhao (✉)

State Key Laboratory for Modification of Chemical Fibers and Polymer Materials, College of Material Science and Engineering, Chemical Fibers Research Institute, Donghua University, Shanghai 201620, People's Republic of China
e-mail: zhyw@dhu.edu.cn

J. Zhao

e-mail: zjxin@dhu.edu.cn

g_{12}	Concentration-dependent binary interaction parameter between non-solvent and solvent
g_{23}	Binary interaction parameter between solvent and polymer
g_{13}	Binary interaction parameter between non-solvent and polymer
ΔG_m	Gibbs free energy of mixing
ΔG^E	Excess Gibbs free energy of mixing
n_1	Molar fraction of non-solvent
n_2	Molar fraction of solvent
R	Gas constant
T	Absolute temperature
$\Lambda_{12}, \Lambda_{21}$	Wilson parameter
ϕ_1	Volume fraction of non-solvent
ϕ_2	Volume fraction of solvent
ϕ_3	Volume fraction of polymer
V_1	Molar volume of non-solvent
V_2	Molar volume of solvent
$\lambda_{12} = \lambda_{21}$	Interaction energy parameter between non-solvent and solvent
λ_{22}	Interaction energy parameter between solvent and solvent
λ_{11}	Interaction energy parameter between non-solvent and non-solvent
γ_1	Activity coefficient of non-solvent
γ_2	Activity coefficient of solvent
$\delta_{1,d}$	Dispersion force component of the solubility parameter of non-solvent
$\delta_{1,p}$	Polar force component of the solubility parameter of non-solvent
$\delta_{1,h}$	Hydrogen bond component of the solubility parameter of non-solvent
$\delta_{3,d}$	Dispersion force component of the solubility parameter of polymer
$\delta_{3,p}$	Polar force component of the solubility parameter of polymer
$\delta_{3,h}$	Hydrogen bond component of the solubility parameter of polymer
$\Delta\mu_1$	Difference between the chemical potential of non-solvent in the mixture and the pure state
$\Delta\mu_2$	Difference between the chemical potential of solvent in the mixture and the pure state
$\Delta\mu_3$	Difference between the chemical potential of polymer in the mixture and the pure state

$\Delta\mu_{1,A}$	Difference between the chemical potential of non-solvent in polymer-rich phase and the pure state
$\Delta\mu_{2,A}$	Difference between the chemical potential of solvent in polymer-rich phase and the pure state
$\Delta\mu_{3,A}$	Difference between the chemical potential of polymer in polymer-rich phase and the pure state
$\Delta\mu_{1,B}$	Difference between the chemical potential of non-solvent in polymer-poor phase and the pure state
$\Delta\mu_{2,B}$	Difference between the chemical potential of solvent in polymer-poor phase and the pure state
$\Delta\mu_{3,B}$	Difference between the chemical potential of polymer in polymer-poor phase and the pure state
$\phi_{1,A}$	Volume fraction of non-solvent in polymer-rich phase
$\phi_{2,A}$	Volume fraction of solvent in polymer-rich phase
$\phi_{3,A}$	Volume fraction of polymer in polymer-rich phase
$\phi_{1,B}$	Volume fraction of non-solvent in polymer-poor phase
$\phi_{2,B}$	Volume fraction of solvent in polymer-poor phase
$\phi_{3,B}$	Volume fraction of polymer in polymer-poor phase
G_{22}	$\frac{\partial^2 \Delta G_m}{\partial (\phi_2)^2}$
G_{33}	$\frac{\partial^2 \Delta G_m}{\partial (\phi_3)^2}$
G_{23}	$\frac{\partial^2 \Delta G_m}{\partial \phi_2 \partial \phi_3}$
G_{222}	$\frac{\partial^3 \Delta G_m}{\partial (\phi_2)^3}$
G_{223}	$\frac{\partial^3 \Delta G_m}{\partial (\phi_2)^2 \partial \phi_3}$
G_{233}	$\frac{\partial^3 \Delta G_m}{\partial \phi_2 \partial (\phi_3)^2}$
u_1	$\phi_1 / (\phi_1 + \phi_2)$
u_2	$\phi_2 / (\phi_1 + \phi_2)$

Abbreviations

PAN	Polyacrylonitrile
DMSO	Dimethyl sulfoxide
LCP	Linearized cloud-point
NG	Nucleation and growth
SD	Spinodal decomposition

Introduction

Polyacrylonitrile (PAN) fiber is the most important precursor for high performance carbon fiber [1], which has a wide variety of applications in civil and engineering fields, for example, in the aerospace and aviation industry. The performance of carbon fiber is strongly sensitive to the microstructure of its precursor PAN fiber, which plays an important role in the pre-oxidation and carbonization treatments [2, 3]. PAN fiber

precursor is generally produced using wet or dry-jet wet spinning technology [4–10]. In wet spinning, after a spinning dope is extruded from spinneret, it enters into a coagulation bath to form nascent fibers. In dry-jet wet spinning, the extruded spinning dope first passes through a short air gap before entering into the coagulation bath. In the coagulation bath, the PAN spinning dope is gradually solidified via phase separation induced by a composition change resulted from the dual diffusions of the solvent and non-solvent. Thus, the coagulation is the key process to control the microstructure and mechanical properties of the resultant fibers. Due to the coexistence of kinetically controlled dual diffusion and thermodynamically controlled phase separation, the coagulation mechanism of spinning dope is very complicated. The construction of a ternary phase diagram will be helpful to the understanding of the thermodynamic phase behavior of the spinning dope during the coagulation process and thus the clarification of the coagulation mechanism.

The phase diagram of a ternary system can be constructed via cloud-point titration method if the viscosity of the solution is low. Unfortunately, polymer solutions used for spinning are of high concentration and high viscosity. Therefore, the Flory–Huggins theory of polymer solution, which was extended to ternary systems containing non-solvent, solvent, and polymer by Tompa, is needed to establish the phase diagram including the binodal curve, spinodal curve, and critical point [11–13].

In this study, ternary systems consisting of PAN, dimethyl sulfoxide (DMSO), and non-solvent (water or ethanol) were investigated. Cloud-point curve was determined via combination of cloud-point titration of dilute PAN solutions with Boom's linearized cloud-point (LCP) correlation [14]. Binary interaction parameters of the systems were calculated from excess Gibbs free energy or solubility parameters. The theoretical ternary phase diagrams were then numerically calculated and optimized via comparison with the cloud-point curve. The effects of the non-solvent species on the phase behavior of PAN spinning dope in the coagulation medium and also the microstructure of PAN nascent fibers were discussed based on the theoretical phase diagrams.

Experiment

Materials

PAN terpolymer (acrylonitrile:methylacrylate:itaconic acid = 95.6:3.4:1.0) was purchased from Shanghai Petrochemical PAN Co. Ltd. with a viscosity-average molecular weight of 7.8×10^4 g/mol. Dimethyl sulfoxide (DMSO) and ethanol of analytical pure grade were purchased from Shanghai Boer chemical reagent Co. Ltd. Deionized water was used in all the experiments.

Determination of the cloud-point curve

The cloud-point data of dilute PAN solutions were experimentally determined by titration method. A series of PAN solutions with concentration of 2.0, 3.0, 4.0, and

5.0 wt% in DMSO were first prepared. The mixture of water/DMSO (70/30) or ethanol/DMSO (70/30) was then slowly added into the PAN solution under magnetic stirring by a microburette. During titration, the temperature of PAN solution was kept at 25 °C. At the first sight of turbidity, the addition of the mixture was stopped, which was followed by another 3 min of stirring. More mixture was added if the solution turned to be clear again; otherwise, it was considered as the cloud-point.

The cloud-points of PAN solutions with high concentrations were calculated based on Boom's LCP correlation for non-solvent/solvent/polymer ternary systems.

Preparation of PAN spinning dope

A certain amount of PAN terpolymer was dispersed in a mixture of water/DMSO (5/95, v/v) in a glass bottle and allowed to successively swell at 50 °C for 2 h and dissolve at 80 °C for 6 h under stirring. After that, the solution was deaerated at 80 °C overnight in a drying oven.

Preparation of PAN Fibers via Wet spinning

The fibers were spun via wet spinning with a self-built experimental spinning apparatus. The dope with a PAN concentration of 22% was passed through a spinneret of six holes (diameter of 0.15 mm) and entered into a coagulation bath containing a mixture of water/DMSO (60/40, v/v) or ethanol/DMSO (60/40, v/v) at 25 °C. The gel fiber samples, just coming out of the coagulation bath, were washed thoroughly with distilled water to remove residual DMSO. After rinsing, the fibers were dried in air for 2 days at room temperature.

Characterization

Mechanical measurement

The mechanical properties of the nascent PAN fibers were measured using a XQ-1 tensile testing machine at a crosshead speed of 10 mm/min with a gauge length of 20 mm. In each case, 15 samples were tested, and the average values of tenacity, breaking elongation, and Young's modulus were obtained. The density of various fibers was determined at 25 °C using the density gradient column method.

SEM analysis

The microstructure of the nascent fibers was examined using a scanning electron microscope (S-3000N). The gel fiber samples were fractured in liquid nitrogen, followed by drying overnight in a vacuum oven at room temperature. The samples were coated with gold in a sputtering device before observation.

Modeling

Binodal curve

According to the extended Flory–Huggins theory, the Gibbs free energy of mixing for a ternary system is described as follows [12]:

$$\frac{\Delta G_m}{RT} = n_1 \ln \phi_1 + n_2 \ln \phi_2 + n_3 \ln \phi_3 + g_{12}n_1\phi_2 + g_{13}n_1\phi_3 + g_{23}n_2\phi_3, \quad (1)$$

where n_i and ϕ_i are the number of moles and volume fraction of component i , respectively, R is the gas constant, T is the absolute temperature, g_{ij} is concentration-dependent binary interaction parameters between component i and j . The subscripts refer to non-solvent (1), solvent (2), and polymer (3). In the present study, only binary interaction parameters are considered; meanwhile, g_{13} and g_{23} are assumed to be concentration independent.

According to the definition of chemical potential, the following three equations are derived:

$$\begin{aligned} \frac{\Delta\mu_1}{RT} &= \ln \phi_1 + 1 - \phi_1 - \frac{V_1}{V_2}\phi_2 - \frac{V_1}{V_3}\phi_3 + (g_{12}\phi_2 + g_{13}\phi_3)(\phi_2 + \phi_3) - \frac{V_1}{V_2}g_{23}\phi_2\phi_3 \\ &\quad - u_1u_2\phi_2\left(\frac{dg_{12}}{du_2}\right), \end{aligned} \quad (2)$$

$$\begin{aligned} \frac{\Delta\mu_2}{RT} &= \ln \phi_2 + 1 - \phi_2 - \frac{V_2}{V_1}\phi_1 - \frac{V_2}{V_3}\phi_3 + \left(\frac{V_2}{V_1}g_{12}\phi_1 + g_{23}\phi_3\right)(\phi_1 + \phi_3) \\ &\quad - \frac{V_2}{V_1}g_{13}\phi_1\phi_3 - \frac{V_2}{V_1}u_1u_2\phi_1\left(\frac{dg_{12}}{du_2}\right), \end{aligned} \quad (3)$$

$$\begin{aligned} \frac{\Delta\mu_3}{RT} &= \ln \phi_3 + 1 - \phi_3 - \frac{V_3}{V_1}\phi_1 - \frac{V_3}{V_2}\phi_2 + \left(\frac{V_3}{V_1}g_{13}\phi_1 + \frac{V_3}{V_2}g_{23}\phi_2\right)(\phi_1 + \phi_2) \\ &\quad - \frac{V_3}{V_1}g_{12}\phi_1\phi_2, \end{aligned} \quad (4)$$

where $\Delta\mu_i$ is the difference between the chemical potential of component i in the mixture and pure state, V_i is the molar volume of component i , $u_1 = \phi_1/(\phi_1 + \phi_2)$, and $u_2 = \phi_2/(\phi_1 + \phi_2)$.

Based on the definition of the binodal curve where the chemical potential of the polymer-rich phase and that of the polymer-poor phase reach equilibrium, there exist equations as follows:

$$\Delta\mu_{i,A} = \Delta\mu_{i,B}, \quad i = 1, 2, 3, \quad (5)$$

where the subscripts A and B refer to the polymer-rich and polymer-poor phases, respectively.

Also, there exists Eq. 6 according to mass conservation law:

$$\sum \phi_{i,A} = \sum \phi_{i,B} = 1, \quad i = 1, 2, 3. \quad (6)$$

Equations 5 and 6 include five coupled nonlinear equations with six unknowns: $\phi_{1,A}$, $\phi_{2,A}$, $\phi_{3,A}$, $\phi_{1,B}$, $\phi_{2,B}$, and $\phi_{3,B}$.

Spinodal curve

The spinodal curve of a ternary system satisfies the following equation [11]:

$$G_{22} \cdot G_{33} = (G_{23})^2. \quad (7)$$

The free energies G_{22} , G_{23} , and G_{33} can be expressed as follows:

$$G_{22} = \frac{1}{\phi_1} + \frac{V_1}{V_2 \phi_2} - 2g_{12} + 2(u_1 - u_2) \left(\frac{dg_{12}}{du_2} \right) + u_1 u_2 \left(\frac{d^2 g_{12}}{du_2^2} \right), \quad (8)$$

$$G_{23} = \frac{1}{\phi_1} - (g_{12} + g_{13}) + \frac{V_1}{V_2} g_{23} + u_2(u_1 - 2u_2) \left(\frac{dg_{12}}{du_2} \right) + u_1 u_2^2 \left(\frac{d^2 g_{12}}{du_2^2} \right), \quad (9)$$

$$G_{33} = \frac{1}{\phi_1} + \frac{V_1}{V_3 \phi_3} - 2g_{13} + 2u_2^2(1 - u_1) \left(\frac{dg_{12}}{du_2} \right) + u_1 u_2^3 \left(\frac{d^2 g_{12}}{du_2^2} \right). \quad (10)$$

Still, the components of ternary system obey the mass conservation law:

$$\sum \phi_i = 1, \quad i = 1, 2, 3. \quad (11)$$

Equations 7 and 11 include two coupled nonlinear equations with three unknowns: ϕ_1 , ϕ_2 , and ϕ_3 .

Critical point

The critical point composition meets the following equation [11]:

$$G_{222} G_{33}^2 - 3G_{223} G_{23} G_{33} + 3G_{233} G_{23}^2 - G_{22} G_{23} G_{33} = 0. \quad (12)$$

Equations 11 and 12 also include two coupled nonlinear equations with three unknowns: ϕ_1 , ϕ_2 , and ϕ_3 . Thus, assuming one of the unknowns as an independent variable, the binodal curve, spinodal curve, and critical point can be calculated using least square method [13] with the help of the nonlinear function of Lsqnonlin in Matlab.

Determination of the thermodynamic parameters

To construct a phase diagram numerically, binary interaction parameters of non-solvent/solvent, solvent/polymer, and non-solvent/polymer are indispensable.

Non-solvent/solvent interaction parameter (g_{12})

In this study, g_{12} was calculated from the excess Gibbs free energy (ΔG^E), which is generally obtained from vapor–liquid equilibrium experiments [15–17].

$$\begin{aligned} \Delta G^E / RT &= \Delta G_m / RT - (n_1 \ln n_1 + n_2 \ln n_2) \\ &= -n_1 \ln(n_1 + \Lambda_{12} n_2) - n_2 \ln(n_2 + \Lambda_{21} n_1), \end{aligned} \quad (13)$$

where Λ_{ij} is the Wilson parameter.

For a binary system:

$$\frac{\Delta G_m}{RT} = n_1 \ln \phi_1 + n_2 \ln \phi_2 + g_{12}n_1\phi_2. \quad (14)$$

From Eqs. 13 and 14, g_{12} can be evaluated as follows:

$$g_{12} = \frac{1}{n_1\phi_2} \left[n_1 \ln \frac{n_1}{\phi_1} - n_1 \ln(n_1 + \Lambda_{12}n_2) + n_2 \ln \frac{n_2}{\phi_2} - n_2 \ln(n_2 + \Lambda_{21}n_1) \right]. \quad (15)$$

It is generally accepted that a good agreement between experimental and theoretical miscible regions can be obtained when g_{12} is considered to be concentration dependent (i.e., $g_{12}(\phi_2)$). There are two function forms of $g_{12}(\phi_2)$ as suggested by Tompa [11] and Koningsveld et al. [15], respectively. Here, Tompa's polynomial form (Eq. 16) was adopted.

$$g_{12}(\phi_2) = a_0 + a_1\phi_2 + a_2\phi_2^2 + a_3\phi_2^3 + a_4\phi_2^4 + \dots \quad (16)$$

For the water/DMSO binary system, the Wilson parameters Λ_{12} and Λ_{21} (see Table 1) were calculated from data of $(\lambda_{12} - \lambda_{11})$ and $(\lambda_{21} - \lambda_{22})$, which were obtained directly from Gmehling and Onken [16], by the following equations:

$$\Lambda_{12} = \frac{V_2}{V_1} e^{-\frac{(\lambda_{12}-\lambda_{11})}{RT}}, \quad (17)$$

$$\Lambda_{21} = \frac{V_1}{V_2} e^{-\frac{(\lambda_{21}-\lambda_{22})}{RT}}. \quad (18)$$

After that, $g_{12}(\phi_2)$ was successively calculated via Eq. 15 and fitted by polynomial with four orders.

For the ethanol/DMSO binary system, as no vapor–liquid equilibrium data are available, the excess Gibbs free energy (ΔG^E) was obtained from activity coefficient of the components (γ_i) according to Eq. 19.

$$\Delta G^E = RT(n_1 \ln \gamma_1 + n_2 \ln \gamma_2). \quad (19)$$

From Eqs. 13, 14, and 19, g_{12} can also be evaluated as follows:

$$g_{12} = \frac{1}{n_1\phi_2} \left(n_1 \ln \frac{n_1}{\phi_1} + n_1 \ln \gamma_1 + n_2 \ln \frac{n_2}{\phi_2} + n_2 \ln \gamma_2 \right). \quad (20)$$

The universal quasi-chemical functional group activity coefficient (UNIFAC) method [17, 18] was employed to calculate the activity coefficients of ethanol and DMSO. Also, the $g_{12}(\phi_2)$ was calculated via Eq. 20 and fitted in polynomial.

The concentration-dependent g_{12} of water/DMSO and ethanol/DMSO systems is presented in Table 2 and Fig. 1. As shown in Fig. 1, g_{12} of both systems decreases

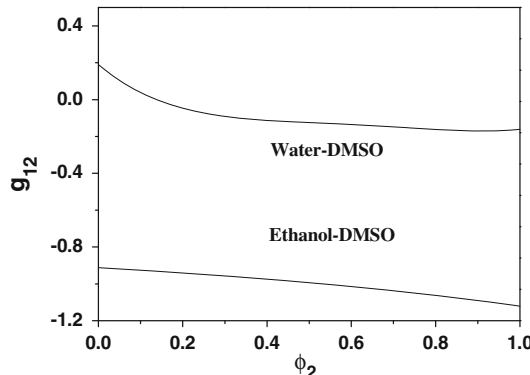
Table 1 Wilson parameter of water/DMSO system

Non-solvent	Solvent	$V_1/\text{mL mol}^{-1}$	$V_2/\text{mL mol}^{-1}$	$\lambda_{12} - \lambda_{11}/\text{J mol}^{-1}$	$\lambda_{21} - \lambda_{22}/\text{J mol}^{-1}$	Λ_{12}	Λ_{21}
Water	DMSO	18	71.3	-241.52	-1665.98	5.9546	0.0152

Subscripts 1 and 2 denote water and DMSO, respectively

Table 2 Concentration-dependent non-solvent/solvent interaction parameters (g_{12}) of water/DMSO and ethanol/DMSO systems

System	g_{12}
Water-DMSO	$0.1899 - 1.9256\phi_2 + 4.6527\phi_2^2 - 5.1585\phi_2^3 + 2.0797\phi_2^4$
Ethanol-DMSO	$-0.9119 - 0.1440\phi_2 + 0.0023\phi_2^2 - 0.0951\phi_2^3 + 0.0274\phi_2^4$

Fig. 1 Concentration-dependent g_{12} of water/DMSO and ethanol/DMSO systems calculated from the excess Gibbs energy of mixing

with the increasing of DMSO fraction. Also, the g_{12} values are usually less than zero, indicating the strong interactions between the components: both water and ethanol form hydrogen bonds with DMSO [19]. Due to the strong non-solvent/solvent interactions, the solvent coming out of the filament is more than the non-solvent entering into the filament during the coagulation process. Thus, the PAN concentration in the filament increases as the coagulation proceeds. The more negative g_{12} value of ethanol/DMSO system means that a larger increase of PAN concentration during the fiber formation, thus, fiber with denser structure is expected to be obtained.

DMSO/PAN (g_{23}) interaction parameter

The solvent/polymer interaction parameter (g_{23}) can be obtained by measuring the activity of the solvent via a variety of methods including osmotic pressure [20], light scattering [21], and gas–liquid equilibrium [22]. Also, Dong et al. [23] determined g_{23} of DMSO/PAN system at different temperatures by intrinsic viscosity measurements according to a simplified Rudin model [24, 25]. Here, Dong's datum, i.e., $g_{23} = 0.21$, was adopted.

Water/PAN and ethanol/PAN (g_{13}) interaction parameters

The water/PAN interaction parameter can be evaluated via simple equilibrium swelling method [26, 27]. However, due to the high volatility of ethanol, the experimental error of the swelling method became fairly large for the ethanol/PAN

Table 3 Three components of δ and molar volume of PAN, water, and ethanol

	$V/\text{mL mol}^{-1}$	$\delta_d/(\text{J cm}^{-3})^{0.5}$	$\delta_p/(\text{J cm}^{-3})^{0.5}$	$\delta_h/(\text{J cm}^{-3})^{0.5}$
water	18.0	15.5	16.0	42.3
Ethanol	58.5	15.8	8.8	19.4
PAN	–	21.7	14.1	9.1

The data were taken from [29]

system. Therefore, we evaluated g_{13} of ethanol/PAN system directly from the Hansen solubility parameters (Eq. 21) [28], which are available in literature. In order to construct phase diagram of the two systems under similar conditions, g_{13} of water/PAN system was also evaluated from the Hansen solubility parameters.

$$g_{13} = \alpha \frac{V_1}{RT} \left[(\delta_{1,d} - \delta_{3,d})^2 + 0.25(\delta_{1,p} - \delta_{3,p})^2 + 0.25(\delta_{1,h} - \delta_{3,h})^2 \right], \quad (21)$$

where δ_d , δ_p , and δ_h are the dispersion force component, polar force component, and hydrogen bond component of the solubility parameter, respectively; α is the correction constant.

According to Eq. 21 and the δ data of water, ethanol, and PAN listed in Table 3, g_{13} of water/PAN and ethanol/PAN systems were calculated without correction (i.e., $\alpha = 1$) to be 2.29 and 1.61, respectively. The smaller g_{13} of ethanol/PAN system as compared with that of water/PAN system also indicates a weaker coagulation ability of ethanol.

Results and discussion

Cloud-point curve

According to the study of Boom et al. [14], if only liquid–liquid demixing occurs for a non-solvent/solvent/polymer ternary system, the cloud-point composition of polymer solutions should be fitted well with LCP correlation as Eq. 22; if both liquid–liquid demixing and liquid–solid demixing occur simultaneously, the disturbing of the latter would result in poor linear correlation of LCP curve:

$$\ln \frac{w_1}{w_3} = b \ln \frac{w_2}{w_3} + a, \quad (22)$$

where w_i is the mass fraction of component i , and a and b are constants.

As shown in Fig. 2, the linear correlation coefficients (R^2) of LCP curves of both water/DMSO/PAN and ethanol/DMSO/PAN systems are above 0.999, indicating that only liquid–liquid demixing occurs in the two systems. In addition, as the non-solvent water is replaced with ethanol, the value of b increases slightly, while that of a (negative value) decreases substantially, suggesting that the coagulation ability of ethanol is weaker as compared with water.

Figure 3 shows the experimental cloud-points and calculated cloud-point curve based on Boom's LCP correction of water/DMSO/PAN and ethanol/DMSO/PAN

Fig. 2 LCP curves of water/DMSO/PAN and ethanol/DMSO/PAN systems based on Boom's LCP correlation

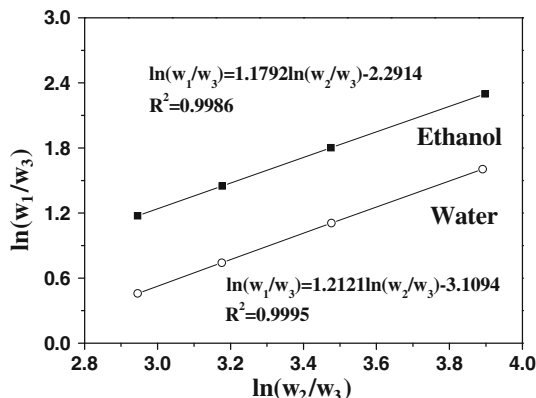
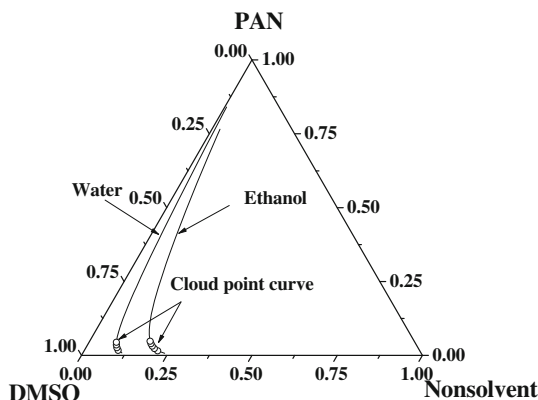


Fig. 3 Cloud-point curve with experimental cloud-points (white open circle) and calculated cloud-point curve based on Boom's LCP correlation of water/DMSO/PAN and ethanol/DMSO/PAN systems



systems. It is clear that as the fraction of PAN increases, the cloud-point curve turns to be closer to the DMSO–PAN side, suggesting that less non-solvent, whether it is water or ethanol, is needed to induce the phase separation of a spinning dope with higher concentration. In addition, as compared with the water/DMSO/PAN system, the cloud-point curve of ethanol/DMSO/PAN system shifts rightwards and moves apart from the DMSO–PAN side, namely, the homogenous region becomes larger, indicating less incompatibility between PAN and ethanol than that between PAN and water. This also means that more ethanol as compared with water is needed to induce the coagulation of PAN under same conditions. Therefore, under same conditions of the coagulation bath (i.e., at the same DMSO concentration and the same temperature of the coagulation medium), the phase separation of the spinning dope is expected to be deferred, which will benefit to the formation of the fiber with uniform microstructure.

Phase diagram of water/DMSO/PAN and ethanol/DMSO/PAN systems

The accuracy of theoretical phase diagram obtained via the numerical calculations based on the extended Flory–Huggins theory strongly depends on the binary

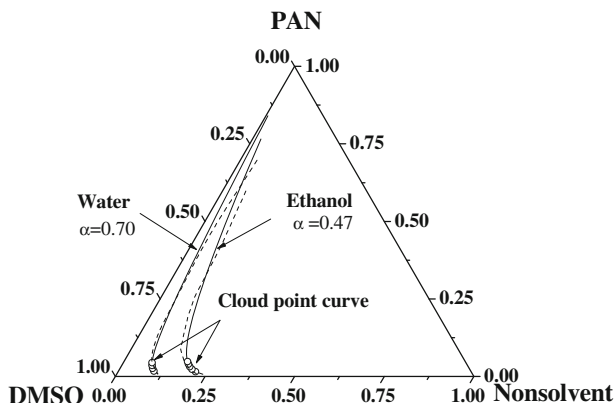


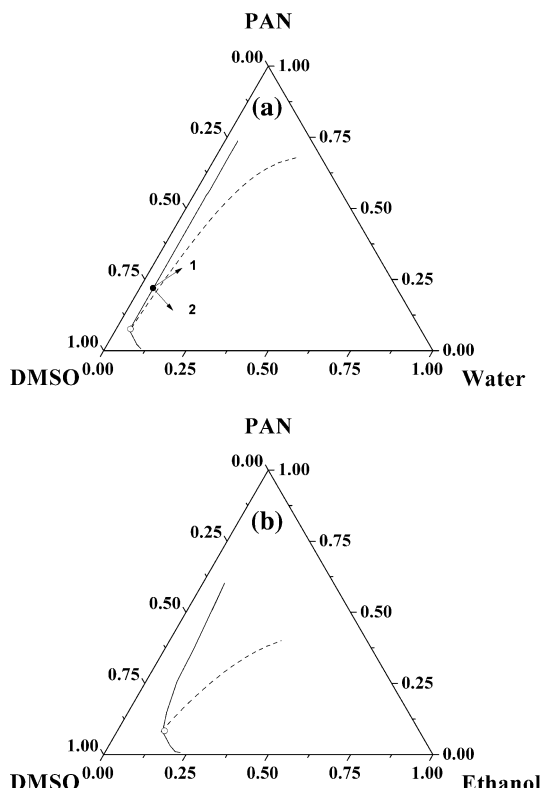
Fig. 4 Comparison of the theoretical binodal curve (*dashed line*) based on the extended Flory–Huggins theory with the cloud-point curve (*thin line*) calculated based on Boom's LCP correlation of water/DMSO/PAN and ethanol/DMSO/PAN systems

interaction parameters. It was reported by Lindvig et al. [28] that the Flory–Huggins interaction parameters estimated from the Hansen parameter can be optimized using correction constant α in Eq. 21. As illustrated in Fig. 4, we can see that after optimization of the g_{13} , the calculated binodal curve agrees well with the cloud-point curve. On this basis, we calculated the theoretical spinodal curve and critical point of the two systems.

Figure 5 illustrates the theoretical binodal curves, spinodal curves, and critical points of water/DMSO/PAN and ethanol/DMSO/PAN systems. As the PAN fractions at the critical point for both systems are very low (less than 10%), far less than the concentration of spinning dope (usually above 20%), hence, during the wet or dry-jet wet spinning process, due to the dual diffusion in the coagulating bath, the spinning dope will enter the meta-stable two-phase region between the spinodal and binodal curves, and nucleation and growth (NG) phase separation occurs at the early stage of fiber-forming process. The NG demixing mechanism will result in the formation of two-phase structure with polymer-poor dispersed phase and polymer-rich continuous phase. In this case, dense and homogenous fiber with small cavity and good mechanical properties will be attained. If the rapid exchange between the solvent and non-solvent turns the dope composition to the unstable two-phase region below the spinodal curve, liquid–liquid phase separation will then take place spontaneously. The spinodal decomposition (SD) demixing mechanism will lead to the formation of an interpenetrating bicontinuous structure. In that case, the resulting fiber is of loose structure with large cavities and poor mechanical properties.

As indicated by Fig. 5, if the non-solvent water is replaced with ethanol, both the miscible region and meta-stable two-phase region enlarge; meanwhile, the unstable two-phase region diminishes. This also suggests that the dope composition during coagulation may stay longer in the meta-stable region. Thus, NG demixing mechanism is favored, and fibers with denser and more homogenous structure and

Fig. 5 The theoretical binodal curve (thin line), spinodal curve (dashed line), and critical point (open circle) of water/DMSO/PAN (a) and ethanol/DMSO/PAN (b) systems at 25 °C (filled circle) represents the composition of the starting spinning dope) based on the extended Flory–Huggins theory



smaller porosity are expected to be obtained using ethanol as the non-solvent of the coagulation medium.

Morphology and mechanical properties of PAN fibers

SEM micrographs of PAN nascent fibers prepared from water/DMSO/PAN and ethanol/DMSO/PAN systems by wet spinning under similar conditions are depicted in Fig. 6. The cross-sectional shape of PAN fiber (Fig. 6a, b) obtained using water or ethanol as the non-solvent is elliptical and circular, respectively. The PAN fiber prepared from water/DMSO/PAN system displays a gradual changing structure (Fig. 6c): a dense thin skin layer with no visible pores, an intermediate dense thin layer with small amount of pores, and a thick core layer with loose network structure and high porosity (Fig. 6e). This indicates NG phase separation occurs in the outer part of the fiber; while SD phase separation in the inner part. For the fiber prepared from ethanol/DMSO/PAN system, there is no visible skin–core structure (Fig. 6d). Also, the inner part of the fiber is homogenous and dense with few of pores (Fig. 6f), indicating that NG demixing mechanism remains throughout the whole fiber.

Usually, due to the good compatibility between the non-solvent and solvent, as well as the high solvent fraction in the starting spinning dope, the solvent diffusing

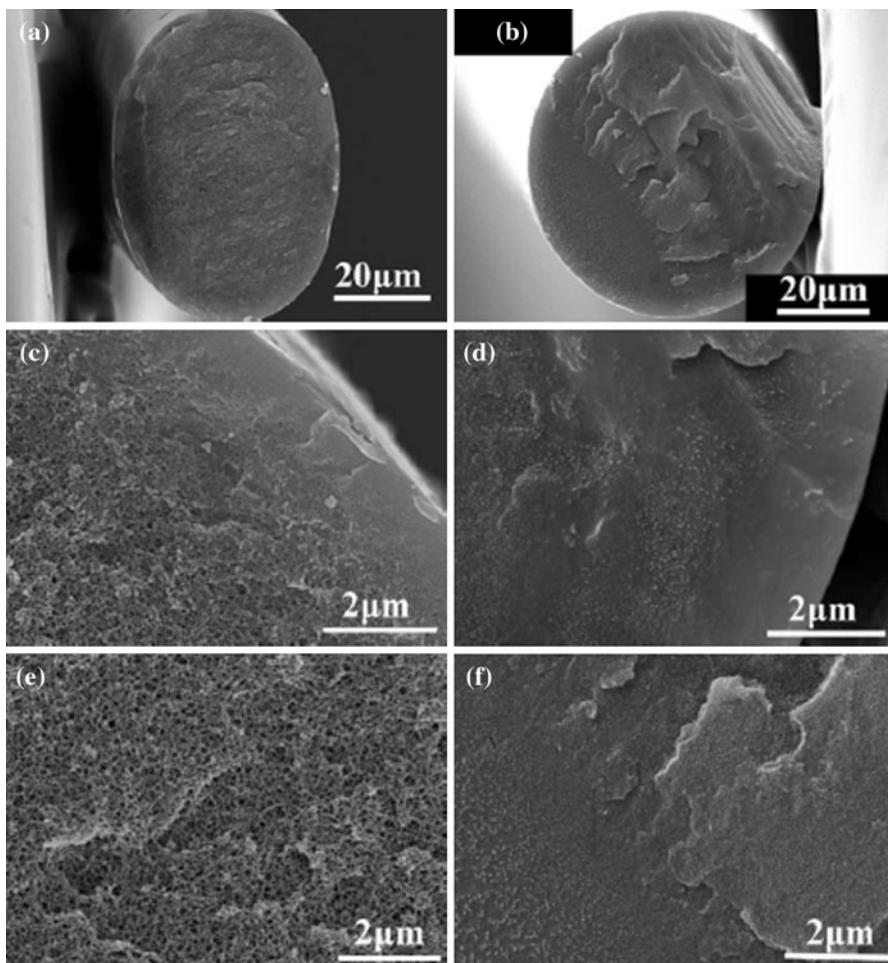


Fig. 6 SEM micrographs of PAN nascent fibers prepared using non-solvent water (**a, c, e**) or ethanol (**b, d, f**)

out of the spinning dope stream is more than the non-solvent diffusing into the dope stream during the coagulation process. The dope composition change follows the route indicated by arrow 1 in Fig. 5a. Thus, NG phase separation occurs in the outer part of the PAN fiber. For the water/DMSO/PAN system, as the composition of the starting PAN spinning dope is located very close to the binodal curve, very minute compositional change would cause the spinning dope stream enter into the unstable region and demix via SD mechanism. Besides, the strong precipitation ability of water causes a quick solidification of the outer part of the fiber, as that is where the dual diffusion initiates, a thin dense skin layer will form. The skin layer will retard the subsequent diffusion of DMSO out of the fiber. As a result, the composition change of the spinning dope will follow the route indicated by arrow 2 (Fig. 5a), the spinning dope would demix via SD mechanism and result in the formation of loose

Table 4 Mechanical properties of nascent PAN fibers prepared using different non-solvents

Non-solvent	PAN fibers			
	Density (g/cm ³)	Tensile strength (cN/dtex)	Breaking elongation (%)	Young's modulus (cN/dtex)
Water	1.12	0.53	108.16	7.21
Ethanol	1.17	0.75	142.13	9.75

network structure with lots of cavities. The evaporation of DMSO and water from the inner part of the fiber causes a deformation in the cross-section of the fiber. As a result, the fiber shape deviated from the circle.

For the ethanol/DMSO/PAN system, the large miscible area leads to a large mixing gap between the composition of starting PAN spinning dope and the theoretical binodal curve. This would retard the solidification of the outer part of the fiber, thus the dual diffusion can occur smoothly throughout the whole fiber. As a result, the composition change of the spinning dope always follows the route 1 (Fig. 5a). In addition, the large meta-stable region also diminishes the possibility of SD phase separation of the spinning dope during the coagulation. Thus, homogeneous and dense PAN fiber with circular cross-section was obtained. As expected, the mechanical properties of the fiber prepared from the water/DMSO/PAN system were poorer, due to its skin–core and high porosity structure (Table 4). Also, the lower density of the fiber obtained using water as the non-solvent confirms its porous structure. Using ethanol as the non-solvent, we could obtain PAN fiber of homogeneous dense microstructure and circular cross-section, and this is the ideal structure of PAN precursor for the production of high performance carbon fibers [30].

Conclusions

For water/DMSO/PAN and ethanol/DMSO/PAN systems, cloud-points of dilute PAN solutions were determined by titration method. The data were fitted well by Boom's LCP correlation, and the cloud-point data of PAN solutions with high concentrations were calculated. The binary interaction parameters of water/DMSO and ethanol/DMSO systems were calculated from the excess Gibbs free energy, while those of water/PAN and ethanol/PAN systems from solubility parameters. Both g_{12} and g_{13} of ethanol/DMSO system have lower values as compared with water/DMSO system. Together with the PAN/DMSO interaction parameter available in literature, the theoretical phase diagrams for the two systems were determined based on the extend Flory–Huggins solution theory. After optimization, the theoretical binodal curve agrees with the cloud-point curve. Using ethanol instead of water as the non-solvent, both the homogeneous region and meta-stable two-phase region become larger in the phase diagram. Fibers using ethanol or water as the non-solvent of the coagulation medium were prepared under similar conditions. Due to the strong coagulation ability of water, the minute gap between

the composition of the starting spinning dope and the binodal curve, as well as the small meta-stable region in the phase diagram, the spinning dope first demixes via NG mechanism and then via SD mechanism during the coagulation, resulting in fibers of core-skin structure and poor mechanical properties. Using ethanol as the non-solvent, the spinning dope demixes via NG mechanism throughout the whole coagulation process, resulting in fibers of homogenous dense structure and good mechanical properties. Thus, high performance PAN fibers can be prepared at a fairly low DMSO concentration of the coagulation medium (i.e., 40%) using ethanol as the non-solvent, dispensing with the gradient coagulation process.

Acknowledgments The authors gratefully acknowledge the financial support from the Science and Technology Commission of Shanghai Municipality (07QA14001) and National 973 Project (2006CB605302 and 2006CB605303).

References

1. Liu XD, Ruland W (1993) X-ray studies on the structure of polyacrylonitrile fibers. *Macromolecules* 26:3030–3036
2. Ogawa H, Saito K (1995) Oxidation behavior of polyacrylonitrile fibers evaluated by new stabilization index. *Carbon* 33:783–788
3. Xu Q, Xu LH, Cao WY, Wu SZ (2005) A study on the orientation structure and mechanical properties of polyacrylonitrile precursors. *Polym Adv Technol* 16:642–645
4. Arbab S, Noorpanah P, Mohammadi N, Soleimani M (2008) Designing index of void structure and tensile properties in wet-spun polyacrylonitrile (PAN) fiber. I. Effect of dope polymer or nonsolvent concentration. *J Appl Polym Sci* 109:3461–3469
5. Arbab S, Mohammadi N, Noorpanah P (2008) Designing index of void structure and tensile properties in wet-spun polyacrylonitrile (PAN) fiber. Part II: Synergistic effect of dope non-solvent concentration and jet draw ratio. *Iran Polym J* 17:227–235
6. Bogun M, Mikolajczyk T, Kurzak A, Blazewicz M, Rajzer I (2006) Influence of the as-spun draw ratio on the structure and properties of PAN fibres including montmorillonite. *Fibers Text East Eur* 14:13–16
7. Bogun M, Mikolajczyk T (2006) Influence of coagulation bath temperature on the porous structure and strength properties of PAN fibres including montmorillonite. *Fibers Text East Eur* 14:19–22
8. Dong XG, Wang CG, Chen J (2007) Study on the coagulation process of polyacrylonitrile nascent fibers during wet-spinning. *Polym Bull* 58:1005–1012
9. Zeng XM, Zhang YW, Zhao JX, Pan D (2007) Investigating the jet stretch in the wet spinning of PAN fiber. *J Appl Polym Sci* 106:2267–2273
10. Zeng XM, Chen JM, Zhao JX, Wu CX, Pan D, Pan N (2009) Investigation the jet stretch in PAN fiber dry-jet wet spinning for PAN–DMSO–H₂O system. *J Appl Polym Sci* 114:3621–3625
11. Tompa H (1956) Polymer solutions. Butterworths Scientific Publications, London
12. Yilmaz L, McHugh AJ (1986) Analysis of nonsolvent–solvent–polymer phase diagrams and their relevance to membrane formation modeling. *J Appl Polym Sci* 31:997–1018
13. Altena FW, Smolders CA (1982) Calculation of liquid–liquid phase separation in a ternary system of a polymer in a mixture of a solvent and a nonsolvent. *Macromolecules* 15:1491–1497
14. Boom RM, Boomgaard VD, Smolders CA (1993) Linearized cloud point curve correlation for ternary systems consisting of one polymer, one solvent and one non-solvent. *Polymer* 34:2348–2356
15. Koningsveld R, Kleintjens LA (1971) Liquid–liquid phase separation in multicomponent polymer systems. X. Concentration dependence of the pair-interaction parameter in the system cyclohexane-polystyrene. *Macromolecules* 4:637–641
16. Gmehling J, Onken U (1977) Chemistry data series. Dechema, Frankfurt
17. Fredenslund A, Jones RL, Prausnitz JM (1975) Group-contribution estimation of activity coefficients in nonideal liquid mixtures. *AIChE J* 21:1086–1099

18. Magnussen T, Rasmussen P, Fredenslund A (1981) UNIFAC parameter table for predication of liquid–liquid equilibria. *Ind Eng Chem Process Des Dev* 20:331–339
19. Noack K, Kiefer J, Leipertz A (2010) Concentration-dependent hydrogen-bonding effects on the dimethyl sulfoxide vibrational structure in the presence of water, methanol, and ethanol. *Chem-PhysChem* 11:630–637
20. Fuoss RM, Mead DJ (1943) Osmotic pressures of polyvinyl chloride solutions by a dynamic method. *J Phys Chem* 47:59–70
21. Zeman L, Tkacik G (1988) Thermodynamic analysis of a membrane-forming system water/N-methyl-2-pyrrolidone/polyethersulfone. *J Membr Sci* 36:119–140
22. Wypych G (2002) Solvent manual. China Petrochemical Industry, Beijing
23. Dong RJ, Keuser M, Zeng XM, Zhao JX, Zhang YW, Wu CX, Pan D (2008) Viscometric measurement of the thermodynamics of PAN terpolymer/DMSO/water system and effect of fiber-forming conditions on the morphology of PAN precursor. *J Polym Sci B* 46:1997–2011
24. Kok CM, Rudin A (1981) Prediction of osmotic pressures of polymer solutions. *J Appl Polym Sci* 26:3575–3582
25. Qian JW, Rudin A (1992) Prediction of thermodynamic properties of polymer solutions. *Eur Polym J* 28:725–732
26. Tan LJ, Pan D, Pan N (2008) Thermodynamic study of a water-dimethylformamide-polyacrylonitrile ternary system. *J Appl Polym Sci* 110:3439–3447
27. Dong RJ, Zhao JX, Zhang YW, Pan D (2008) Morphology control of polyacrylonitrile(PAN) fibers by phase separation technique. *J Polym Sci B* 47:261–275
28. Lindvig T, Michelsen ML, Kontogeorgis GM (2002) A Flory–Huggins model based on the Hansen solubility parameters. *Fluid Phase Equilibr* 203:247–260
29. Hansen CM (2007) Hansen solubility parameters: a user's handbook, 2nd edn. CRC Press, New York, NY
30. Zhang WX, Liu J, Wu G (2003) Evolution of structure and properties of PAN precursors during their conversion to carbon fibers. *Carbon* 41:2805–2812